Numerical and Analytical Modeling of the High-Field Electron Mobility in Strained Silicon

S. Dhar, G. Karlowatz, E. Ungersboeck and H. Kosina
Institute for Microelectronics, TU Wien, Gußhausstraße 27–29/E360, 1040 Wien, Austria
Phone: +43-1-58801/36018, Fax: +43-1-58801/36099
E-mail: dhar@iue.tuwien.ac.at

***Abstract*— We have performed a detailed analysis of the electron transport at high electric field in strained Si for different field directions and stress/strain conditions using Full-band Monte Carlo simulations. A phenomenological model describing the velocity-field relationship for electrons in biaxially or uniaxially strained Si has been developed. The model is suitable for incorporation into any device simulator for performing TCAD tasks.**

I. Introduction

The introduction of strain in Si channels, resulting in significant mobility enhancements, is becoming increasingly important for developing next generation CMOS technologies. The strain in Si can be generated either globally, using an epitaxial layer on a relaxed substrate [1][2][3], by mechanical stressing [4][5], or can be induced during the processing steps [6][7].

Biaxially strained Si layers (two surface dimensions being stressed) using relaxed SiGe substrates have shown large enhancements of electron mobility but suffer from several integration issues. There has thus been a interest towards uniaxially straining Si (one surface dimension stressed) which not only enhances the electron mobility but also exhibits superior hole mobility enhancements for PMOS devices [8].

In this work, we studied electron high-field transport in strained Si using Full Band Monte Carlo (FBMC) simulations. The band structure of strained Si was calculated using the empirical pseudopotential method [9] for biaxial tensile strain and uniaxial stress along the substrate normal. A [100] substrate is considered. We propose an empirical model to describe the velocity-field relationship as obtained from FBMC simulations.

II. Monte Carlo Results

Fig. 1 and Fig. 2 show the velocity-field characteristics as obtained from FBMC simulations for biaxially strained Si grown on a relaxed SiGe substrate for different Ge content and field along [100] and [001] directions, respectively. The figures show an increase (decrease) in the total velocity with increasing strain for field along [100] ([001]) direction. For the [100] field direction, the total velocity shows a region of small negative differential mobility. The velocity-field characteristics shown in Fig. 2 exhibit an untypical form for high strain levels. This phenomenon can be explained by the repopulation of valleys induced by the field. The velocity-field curve in Fig. 2

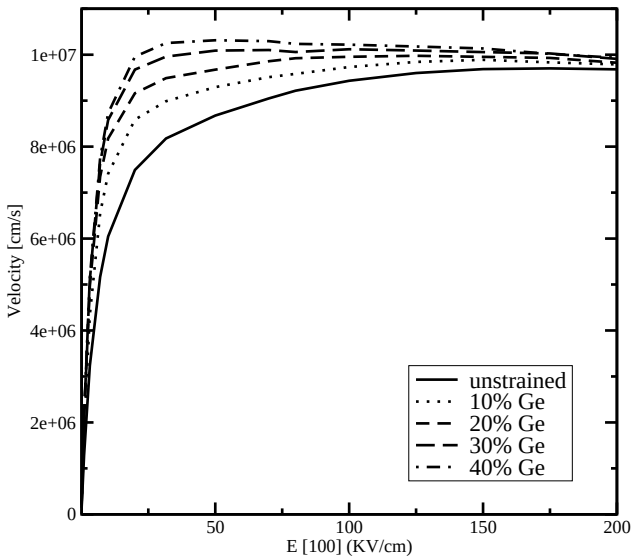

Figure 1: Electron velocity versus field (along [100]) in strained Si on SiGe with increasing Ge content obtained from MC simulations.

is associated with the Δ_2 valleys which move down in energy with increasing strain and have the longitudinal mass in the field direction. These valleys are located at a scaled distance of 0.85 and 1.15 from the center of the first Brillouin zone and are separated by an energy barrier of 129 meV at the X-point as shown in Fig. 3. Repopulation effects within this double valley together with the high population of the double valley, lead to the particular shape of the $v(E)$ curve.

III. Low field mobility

A key parameter in the modeling of the field dependent mobility is the accurate determination of the low-field mobility. Strain induced enhancement of the low-field mobility can be attributed to two complementary effects. Firstly, the intervalley phonon scattering is reduced due to decreased number of final available states. Secondly, due to the energy lowering of the Δ_2 valleys, the electrons prefer to occupy this valley and therefore experience a lower in-plane effective conductivity mass.

The low-field mobility for electrons in strained Si can be calculated using the model developed in [10]. It describes the mobility tensor for electrons in strained Si layers as a function

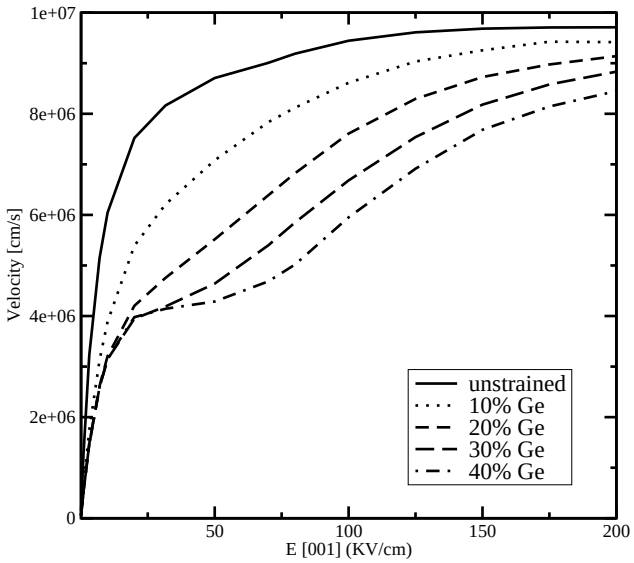

Figure 2: Electron velocity versus field (along [001]) in strained Si on SiGe with increasing Ge content obtained from MC simulations.

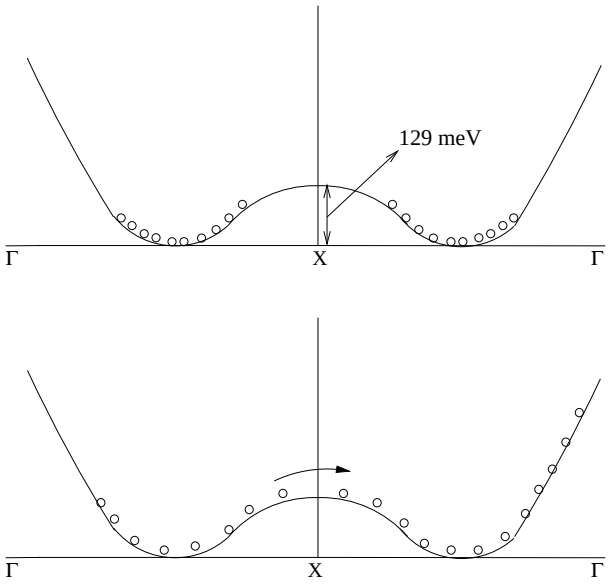

Figure 3: Repopulation effect within the double valley in the equilibrium state (top) and at high-field (bottom)

of strain. It includes the effect of strain-induced splitting of the conduction band valleys in Si, inter-valley scattering, doping dependence and temperature dependence.

The variation of the in-plane mobility with increasing strain for biaxially strained Si, as calculated from MC simulations and the analytical model is shown in Fig. 4. Tensile strained Si enhances the electron mobility whereas compressive strain results in a reduced mobility. There is a minimum in the mobility occurring for the case of compressively strained Si. This can be explained by the interplay between the increased conductivity mass of the Δ_4 valleys (which move down in energy for compressive strain) in the transport direction, and the decreasing inter-valley scattering.

IV. HIGH FIELD MODEL

The high field behavior is modeled using direct fits of empirical expressions to the MC data. This approach has been chosen after a more physically-based, three-valley model had been investigated. However, one problem of such model would be its complexity. For instance, a nonlinear system for nine unknowns, namely the valley populations, valley velocities and valley temperatures, would have to be solved numerically. The peculiar shape of the $v(E)$ curves in Fig. 2 would pose another problem. While the physically-based high-field model could deal with arbitrary strain conditions, the chosen empirical model can not. Therefore, we restricted our study to such strain conditions where only one pair of X-valleys is shifted with respect to the four-fold degenerate X-valleys. These conditions include biaxial stress and uniaxial stress applied along the principal axes of the crystal ($\{100\}$ directions for Si).

If the velocity is governed by the transversal mass m_t, the velocity along the field direction is modeled phenomenologically using the expression

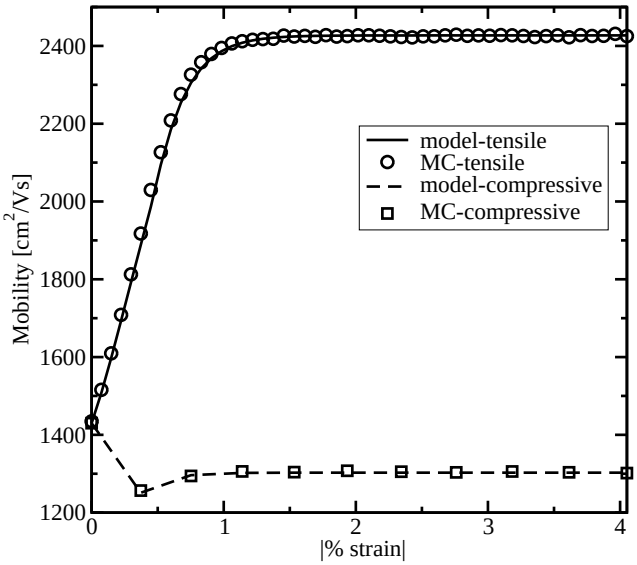

Figure 4: Variation of in-plane mobility for biaxial tensile and compressively strained Si with increasing strain.

$$v(E) = \frac{2\mu_0 E}{1 + \left[1 + \left(\frac{2\mu_0 E}{v_s - m \cdot E}\right)^{\beta}\right]^{1/\beta}}. \qquad (1)$$

This expression is an extension of the standard mobility model used in [11]. Here μ_0 is the low field mobility and v_s is the saturation velocity. The parameter β governs the velocity transition from low to high fields whereas m accounts for the small negative differential mobility occurring in strained Si for higher strain levels.

If the velocity is governed by the longitudinal mass, m_l,the velocity along the field direction is modeled using the expression

$$v(E) = \frac{2\mu_0 E}{1+\left[1+\left(\frac{2\mu_0 E}{v_s(1-\xi)}\right)^{\beta}\right]^{1/\beta}} + v_s\xi\frac{(E/E_0)^{\gamma}}{1+(E/E_0)^{\gamma}} \quad (2)$$

The additional term incorporated in (2) models the velocity kink occurring due to repopulation effects within the X-valleys. The parameter $\xi < 1$ is used to signify the velocity plateau occurring approximately at $v_s(1-\xi)$. E_0 and γ are fit parameters. The empirical dependences of all parameters on the valley splitting are described by simple analytic expressions. In all cases a linear or quadratic expression is sufficient, except for ξ, which is modeled by a rational expression.

$$\xi = \frac{\Delta E/\xi_0}{1+(\Delta E\cdot\xi_1/\xi_0)^2} \quad (3)$$

Here, ξ_0 and ξ_1 are constants. The parameter variation for biaxially tensile strained Si and [001] field direction are plotted in Fig 5.

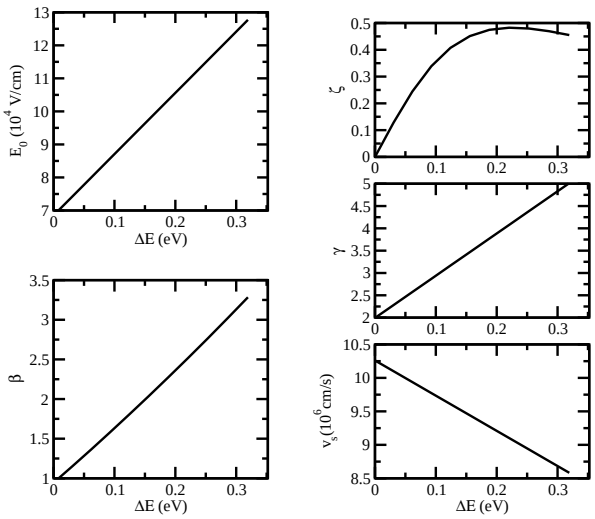

Figure 5: Variation of parameters with strain induced valley splitting for biaxially tensile strained Si and field along [001] direction.

Fig. 6 shows the $v(E)$ characteristics for unstrained Si and strained Si on $Si_{0.6}Ge_{0.4}$ as obtained from the MC simulations and from our model. Biaxial tensile strain increases (decreases) the in-plane (out-of-plane) electron velocity for the complete field range shown. Fig. 7 shows the $v(E)$ characteristics for a 1GPa stressed Si layer for field along [100]. From this figure it can be seen that the application of a uniaxial compressive stress also enhances the in-plane velocity. Conversely, applying uniaxial tensile stress results in an enhanced out of plane

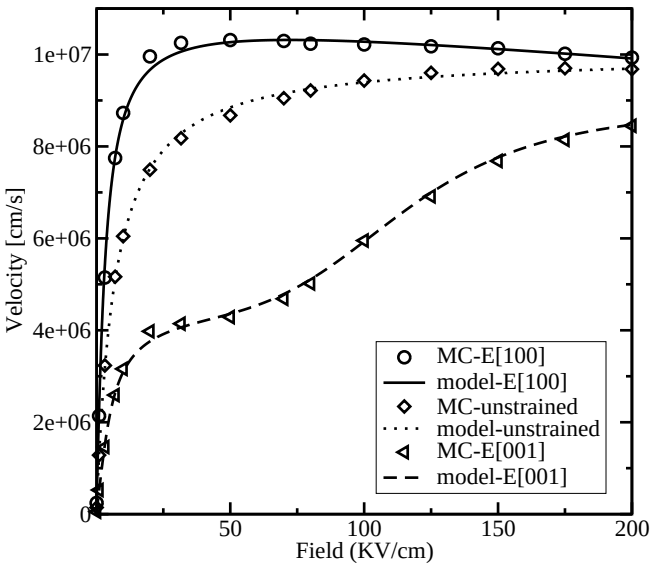

Figure 6: Electron velocity versus field characteristics for unstrained Si and strained Si on $Si_{0.6}Ge_{0.4}$.

velocity, as shown in Fig. 8. The $v(E)$ characteristics for the [111] field directions is shown in Fig. 9 and . From the figure it is observed that for [111] field direction, there is almost no change in the $v(E)$ characteristics for tensile and compressively strainer Si. Fig. 10 shows the $v(E)$ characteristics for [110] field direction. It is observed that this field direction gives the highest electron velocity in comparison to [100] and [111] directions.

V. Conclusion

We have investigated the high-field transport behavior in strained Si for different field directions and stress/strain conditions using FBMC simulations. A phenomenological approach to describe the velocity-field characteristics has been proposed which shows good agreement with the simulations results. The explicitness of the model enables its implementation into any conventional device simulator for performing TCAD tasks.

Acknowledgment

This project has been supported in parts by the European Commission, NoE SINANO, IST-506844, and NoE TARGET, IST-1-507893.

References

[1] J. Welser, J. Hoyt, and J. Gibbons, in *IEDM Tech.Dig.* (1992), pp. 1000–1002.

[2] K. Rim, J.-L. Hoyt, and J.-F. Gibbons, in *IEDM Tech.Dig.* (1998), pp. 707–710.

[3] J.-L. Hoyt *et al.*, in *IEDM Tech.Dig.* (2002), pp. 23–26.

[4] A. Lochtefeld and D. Antoniadis, IEEE Electron Device Lett. **22**, 591 (2001).

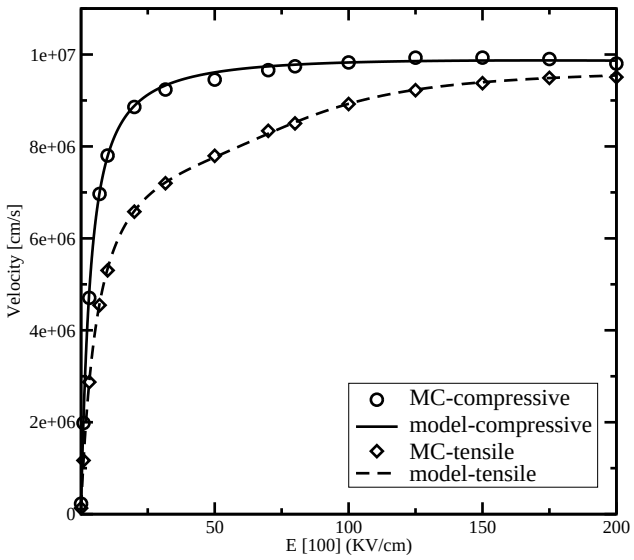

Figure 7: Electron velocity versus field characteristics for Si under uniaxial stress (1GPa) along [001] and field along [100].

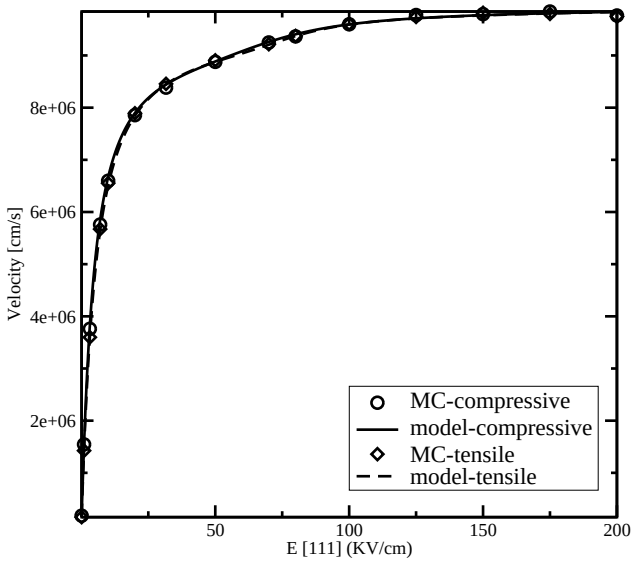

Figure 9: Electron velocity versus field characteristics for Si under uniaxial stress (1GPa) along [001] and field along [111].

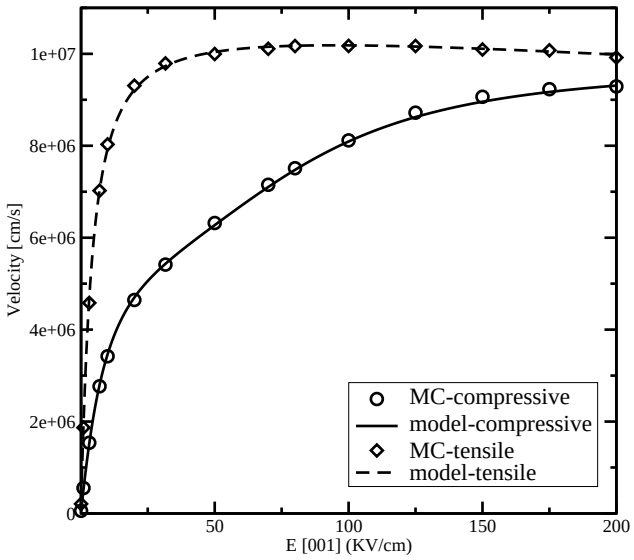

Figure 8: Electron velocity versus field characteristics for Si under uniaxial stress (1GPa) along [001] and field along [001].

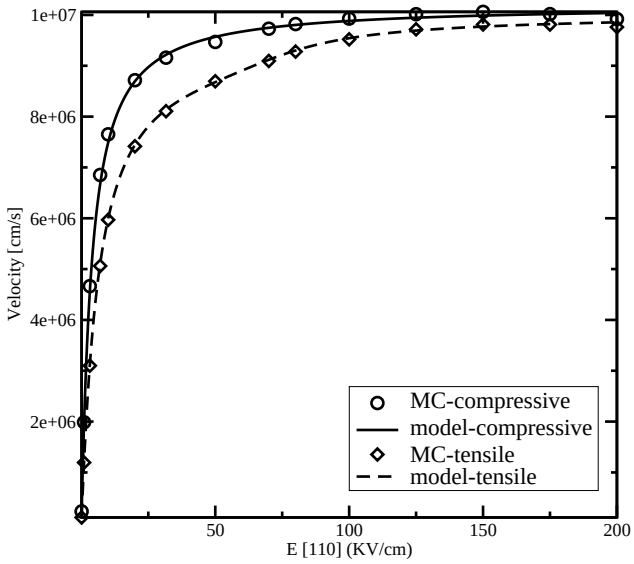

Figure 10: Electron velocity versus field characteristics for Si under uniaxial stress (1GPa) along [001] and field along [110].

[5] S. Maikap *et al.*, IEEE Electron Device Lett. **25**, 40 (2004).

[6] A. Shimizu *et al.*, in *IEDM Tech.Dig.* (2001), pp. 433–437.

[7] S. Ito *et al.*, in *IEDM Tech.Dig.* (2000), pp. 247–251.

[8] K. Uchida *et al.*, in *IEDM Tech.Dig.* (2004), pp. 229–232.

[9] M. Rieger and P. Vogl, Phys.Rev.B **48**, 14276 (1993).

[10] S. Dhar *et al.*, IEEE Trans.Electron Devices **52**, 527 (2005).

[11] Binder *et al., MINIMOS-NT Device and Circuit Simulator, User's Guide, Release 2.0,* Institut für Mikroelektronik, TU Wien, 2002, http://www.iue.tuwien.ac.at/mmnt.